Optics Communications 442 (2019) 40–45

Contents lists available at ScienceDirect

Optics Communications

journal homepage: www.elsevier.com/locate/optcom

Effect of beam profile and partial coherence on coherent beam combining performance

Jan K. Jabczynski *, Przemyslaw Gontar

Institute of Optoelectronics, Military University of Technology, 00-908 Warsaw ul gen. S. Kaliskiego 2, Poland

ARTICLE INFO

Keywords:
Lasers
Laser optics
Laser beams
Coherent beam combining
Partial coherence

ABSTRACT

A numerical model of a coherent beam composed of a two-dimensional array of laser beams was developed; the model enables analysis of random phase mismatch in the combined system, as well as analysis of the influence of atmospheric turbulence. The negative impact of the beam profile, filling factor, and average inter-beam coherence was analyzed. This analysis reveals parametric ranges in which performance metrics decrease by less than 20% of their peak values. Ensuring partial coherence was the most challenging task.

1. Introduction

Since the introduction of lasers, the race toward higher-energy and higher-power near-diffraction-limited laser beams has commenced [1–7]. However, several physical effects (such as thermo-optical effects, Brillouin scattering, Raman scattering, and material damage) were found to limit the power of single-aperture beams [5–7]. By some accounts, during the last decade continuous wave power has been nearing its technological and physical limits for single-mode solid-state lasers. Power values of 15 kW and 10 kW were obtained for solid-state lasers based on bulk crystals [8] and fiber lasers [9], respectively. Moving beyond 100 kW requires a paradigm change. The promises associated with the development of high-power, diode-pumped alkali lasers have not been realized up to now [10,11]; however, the potential advantages are quite evident.

Beam-combining techniques, being the subject of intense theoretical and experimental investigations during the last two decades (see e.g. [12–17]), constitute an alternative approach. These techniques, in principle, can be divided into two categories: (1) those that use serial devices with a single-aperture output and (2) those that use parallel devices with a "*tiled*" aperture, composed of a two-dimensional (2D) array of laser beams. In the case of incoherent summation with single-aperture outputs, polarizing beam combination (PBC) and spectral beam combination (SBC) can be applied. The latter approach has yielded power values above 30 kW in 2015 [14]; however, some fundamental barriers have been identified as well. In the case of parallel (or "*tile*") summation, incoherent beam combination (ICBC) and coherent beam combination (CBC) techniques were suggested. In the ICBC approach, the far-field power density is proportional to N (the number of emitters). Such systems were experimentally demonstrated and were found to be feasible with respect to long propagation distances in the atmosphere [17–20].

According to a simple physical model of the CBC system [12], maximal intensity along the propagation axis is proportional to N^2. However, owing to the lattice architecture, as well as beam profile and technical imperfections, realistic estimates of the averaged power density in the far field can be much lower. Thus, a question arises whether the CBC makes sense and whether it can outperform the ICBC. This question was considered in several works [12,13,15,16], but no definite conclusion has been reached.

The objective of this work was to devise a simple semi-analytical tool to address the above question. We are not concerned here with physical and technical challenges associated with coherent phasing of 2D laser beam arrays in the near field. We propose to look at this problem from the point of view of laser optics, i.e., to define adequate performance metrics of such systems by analyzing the properties of 2D laser beam arrays in the far field. In Section 2, we describe the method and the performance metrics. In Sections 3 and 4, we analyze the impact of several factors: geometry, beam profile, and random phase errors, on the performance of the CBC system.

2. Model

2.1. Beam array architecture

The incident 2D array consists of N beams arranged in a periodical hexagonal lattice (Fig. 1). The amplitude of the incident beam can be defined as follows:

$$A_{source,p}(x,y) = \sum_{l=1}^{N} A_{nf,p}\left(x - a\beta_{x,l}, y - a\beta_{y,l}\right) \quad (1)$$

* Corresponding author.
E-mail address: jan.jabczynski@wat.edu.pl (J.K. Jabczynski).

https://doi.org/10.1016/j.optcom.2019.02.063
Received 31 December 2018; Received in revised form 19 February 2019; Accepted 25 February 2019
Available online 6 March 2019

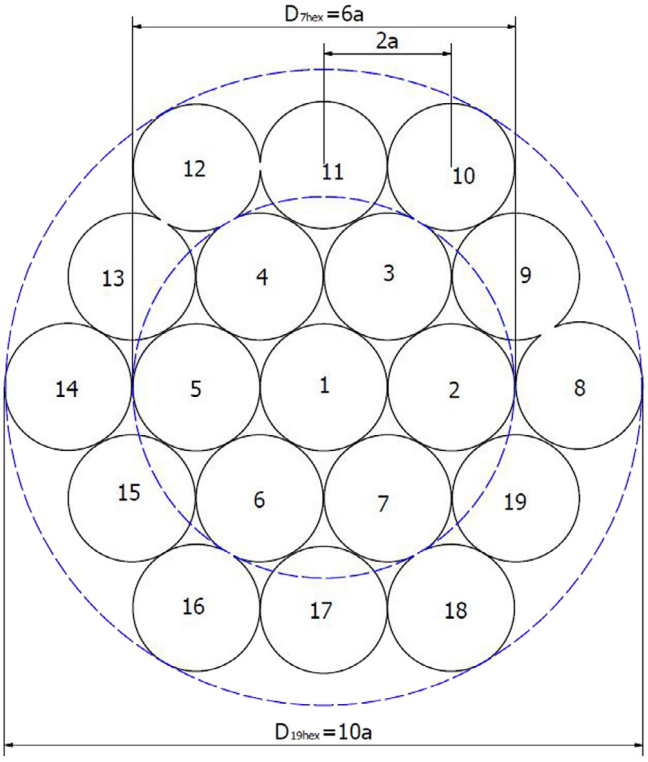

Fig. 1. Structure of 7 and 19 hexagonal lattice.

where a is the half period of the lattice and ($a\beta_{x,l}$, $a\beta_{y,l}$) are the coordinates of the center of lth beam. To analyze the impact of the beam profile, we use the following normalized super-Gaussian functions:

$$A_{nf,p}(r, w_p) = A_{0,p} \exp\left[-(r/w_p)^{2p}\right] \tag{2}$$

Each beam is normalized such that it contains the (1 - ε) power in the circle of the aperture radius $a_* c$, where c is the filling factor and ε is the truncation loss.

$$A_{0,p} = \left((1-\varepsilon)\left(2\pi \int_0^{a\cdot c} \exp\left[-2(r/w_p)^{2p}\right] r dr\right)^{-1}\right)^{1/2} \tag{3}$$

The function $A_{nf,p}(x,y)$ corresponds to a "*top hat*" beam for p = 0, and to a Gaussian beam for p = 1. The effect of truncation is not considered, by taking the highest w_p, such that the truncation loss ε outside of the circle with the diameter 2ac is below 0.001.

2.2. Far field analysis

We focus here on the averaged intensity distributions in the far field, neglecting issues such as beam wandering in the atmosphere and random tilts between beams. To approximate the physical problem of focusing of such a beam array to a long distance f, we used here unidimensional angular coordinates (α_x , α_y), defined as follows:

$$\alpha_x = \theta_x D/\lambda = x_{ff} D/\lambda f \quad ; \quad \alpha_y = \theta_y D/\lambda = y_{ff} D/\lambda f \tag{4}$$

where D is the aperture diameter of the array, λ is the wavelength, ($\theta_x = x_{ff}/f$, $\theta_y = y_{ff}/f$) is a pair of angular coordinates in the far field, corresponding to the (x_{ff} , y_{ff}) point in the focal plane, and f is the focal length (the range to a target). Let us note that, the sub-aperture diameter 2a and range f should be chosen such that the Fresnel range of the CBC system is $a^2/\lambda > f$, for effectively increasing the averaged intensity in the far field.

Let us consider first two ideal, opposite cases: CBC and ICBC. In the CBC case, using the Fourier transform properties [13,21], the amplitude function in the far field $A_{ff,\mathrm{CBC},p}$ is given by:

$$A_{ff,\mathrm{CBC},p}(\alpha_x, \alpha_y) = A_{ff,p}(\alpha_x, \alpha_y) \sum_{l=1}^{N} \exp\left[i2\pi\left(\beta_{x,l}\alpha_x + \beta_{y,l}\alpha_y\right) a/D\right] \tag{5}$$

where $A_{ff,p}(\alpha_x, \alpha_y)$ is the Fourier transform of the amplitude function $A_{nf,p}(x, y)$.

The intensity for the fully coherent case is given as follows:

$$I_{ff,\mathrm{CBC},p}(\alpha_x, \alpha_y) = I_{ff,p}(\alpha_x, \alpha_y) \left| \sum_{l=1}^{N} \exp\left[i2\pi\left(\beta_{x,l}\alpha_x + \beta_{y,l}\alpha_y\right) a/D\right] \right|^2 \tag{6}$$

where

$$I_{ff,p}(\alpha_x, \alpha_y) = \pi (ca/\lambda f)^2 \left| A_{ff,p}(\alpha_x, \alpha_y) \right|^2 \tag{7}$$

It is easy to show that the maximal intensity along the axis ($\alpha_x = 0$, $\alpha_y = 0$) is proportional to $(N)^2$ in the CBC case. The diameter of the central zero diffraction mode of a coherently summed 2D beam matrix is much smaller, compared with the diameter of the Fourier image of a single beam. As was shown in Sections 3 and 4, the power content inside diffraction limit circle, which can be precisely determined, depends on the lattice parameters, filling factor, beam profile and partial coherence state between emitters.

In the case of ICBC, assuming perfect intensity summation (without tilt errors), we have for the far field exactly the same distribution as for a single beam multiplied by N:

$$I_{ff,\mathrm{ICBC},p}(\alpha_x, \alpha_y) = N \cdot I_{ff,p}(\alpha_x, \alpha_y) \tag{8}$$

Let us note that for large p the distribution is nearly "*top hat*".

2.3. Model of partial coherent beam combining

The main innovation of the proposed approach is a model of partially coherent beam combining (PCBC). We assume that in the far field the averaged partial coherence between any pair of incident beams is known *a priori*. Thus, the averaged intensity of PCBC in the far field, $I_{ff,PCBC,p}$, is given by:

$$I_{ff,PCBC,p}(\alpha_x, \alpha_y) = I_{ff,p}(\alpha_x, \alpha_y) \sum_{l'=1}^{N} \sum_{l=1}^{N} \gamma_{l,l'} \times \cos\left[2\pi\left(\alpha_x\left(\beta_{x,l} - \beta_{x,l'}\right) + \alpha_y\left(\beta_{y,m} - \beta_{y,m'}\right)\right) a/D\right] \tag{9}$$

where $\gamma_{l,l'}$ is the matrix of mutual coherence coefficients between (l) and (l') beams, satisfying the following relation:

$$\left|\gamma_{l,l'}\right| \le 1 \tag{10}$$

It is easy to show that for CBC $\gamma_{l,l'} = 1$, while for ICBC $\gamma_{l,l'} = \delta_{l,l'}$ (Kronecker's delta).

The factorization in Eq. (9) allows to perform separate analysis with the particular parameters of interest for the incident beam (diameter, fill factor, beam profile) as the arguments of the first component, whereas the phase relations between the beam components are included in the second one. Thus, we first analyze the impact of the beam profile and the filling factor. Further taking into account the phase relations between the beams as determined by the partial coherence parameter, combined analysis can be performed.

The two different approaches for determining $\gamma_{l,l'}$ can be considered.

In the first case, to define the partial coherence matrix $\gamma_{l,l'}$, we assume that the averaged phase error is space-dependent (i.e., the error increases with increasing the distance between emitters), and satisfies the following relation:

$$\gamma_{l,l',var,phase} = \mu_1^{\Delta_{l,l'}{}^{i_{coh}}} \tag{11}$$

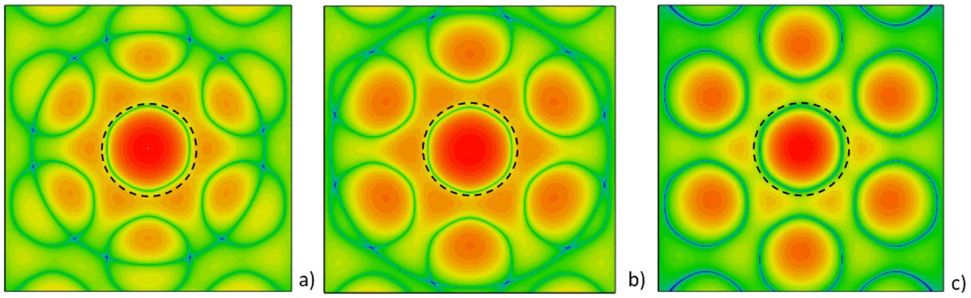

Fig. 2. 2D intensity distributions in logarithmic scale in the far field for (a) $p = 0$, (b) $p = 4$, and (c) $p = 1$. For $\mu_0 = \mu_1 = 1$, dashed circles show the diffraction limit at $1.5\lambda/D$.

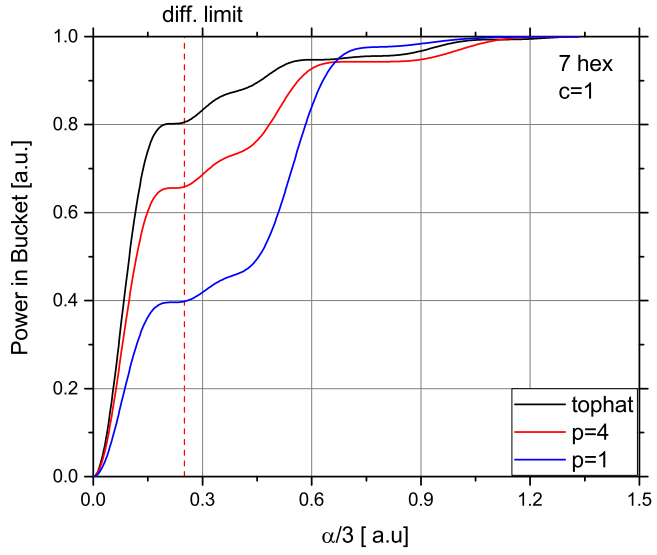

Fig. 3. PIB vs angular coordinate for profiles $p = 0$, 1, 4. The filling factor is $c = 1$, the lattice is a 7-hexagonal lattice. The dashed vertical line corresponds to the diffraction limit at $1.5\lambda/D$.

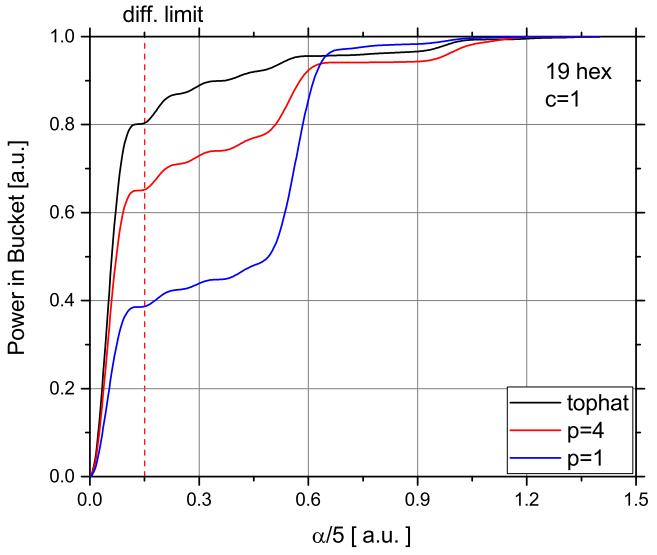

Fig. 4. PIB vs angular coordinate for profiles $p = 0$, 1, 4. The filling factor is $c = 1$, the lattice is a 19-hexagonal lattice. The dashed vertical line corresponds to the diffraction limit at $1.5\lambda/D$.

where $\Delta_{l,l'}$ is the relative distance between centers l, l', defined by :

$$\Delta_{l,l'}, = \sqrt{\left(\beta_{x,l} - \beta_{x,l'}\right)^2 + \left(\beta_{y,l} - \beta_{y,l'}\right)^2} \tag{12}$$

and μ_1 is defined by:

$$\mu_1 = \exp\left(-\left(2a/\rho_0\right)^{i_{coh}}\right) \tag{13}$$

and ρ_0 is the coherence radius (i.e., distance at which the value of the partial coherence coefficient drops to $1/e$), i_{coh} is the index of power describing the model of partial coherence ($i_{coh,5/3} = 11/3 - 2 = 5/3$ for the "*5/3 index law*" of atmospheric turbulence, according to the Kolmogorov model [22,23]), and $i_{coh,G-Sch} = 2$ for Gauss–Schell model of partial coherence [24].

In the second, opposite, case, we assume that $\gamma_{l,l'}$ is space-invariant (i.e., every pair of emitters excluding itself exhibits the same relative root-mean-squared (RMS) phase error σ_0). Then, we obtain the following relation:

$$\gamma_{l,l',inv,phase} = \mu_0^{1-\delta_{l,l'}} \tag{14}$$

where

$$\mu_0 = \exp\left(-\left(2\pi\sigma_0\right)^2\right) \tag{15}$$

This case describes a random phase mismatch between incident beams in the near field.

In practice, for CBC systems with long propagation distances, we deal with a superposition of both effects. Assuming that both phase mismatch processes are independent random variables, the effective partial coherence coefficient $\gamma_{l,l',efc}$ can be defined as follows:

$$\gamma_{l,l',efc} = \gamma_{l,l',var,phase}\,\gamma_{l,l',inv,phase} = \mu_0^{1-\delta_{l,l'}}\,\mu_1^{\Delta_{l,l'}{}^{i_{coh}}} \tag{16}$$

The analysis performed in Sections 3 and 4 allows us to take into account all of these factors. Before proceeding with the analysis, let us introduce the set of CBC performance metrics.

2.4. CBC performance metrics

To analyze and compare scenarios across several geometries and beam profiles, we have to calculate the **P**ower in **B**ucket **D**istribution (PIB) first, according to the following equation:

$$PIB_p\left(\alpha_r\right) = \int_0^{\alpha_r}\int_0^{2\pi} I_{ff,PCBC,p}\alpha d\alpha d\varphi \Big/ \int_0^{\infty}\int_0^{2\pi} I_{ff,PCBC,p}\alpha d\alpha d\varphi \tag{17}$$

Taking into account the previous works on CBC [12,13], the following complimentary suite of the CBC performance metrics is proposed here, which is typical for the laser engineering approach [25] and current analysis:

- Strehl Ratio *SR*, defined as the relative intensity along the axis, normalized to 1 for CBC, "*top hat*" and c = 1 and a given lattice

$$SR = I_{ff,PCBC,p}\left(0,0\right) = I_{ff,p}\left(0,0\right)\sum_{l'=1}^{N}\sum_{l=1}^{N}\gamma_{l,l'} \tag{18}$$

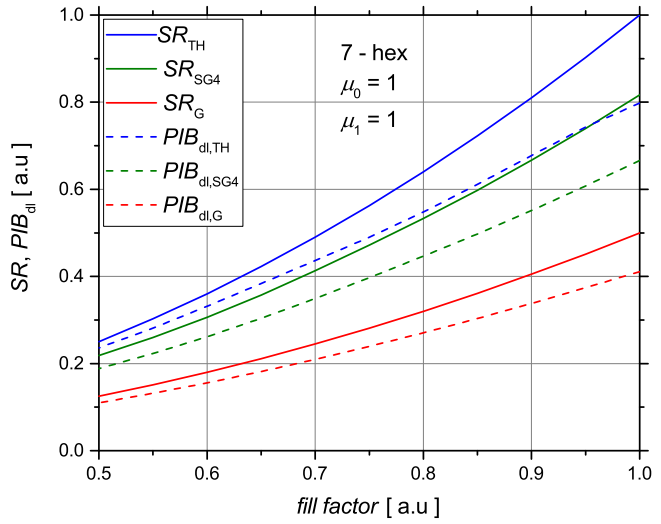

Fig. 5. Strehl ratio SR, combining efficiency PIB_{dl} vs filling factor, for three profiles ($p = 0,\ 1,\ 4$); 7-hex.

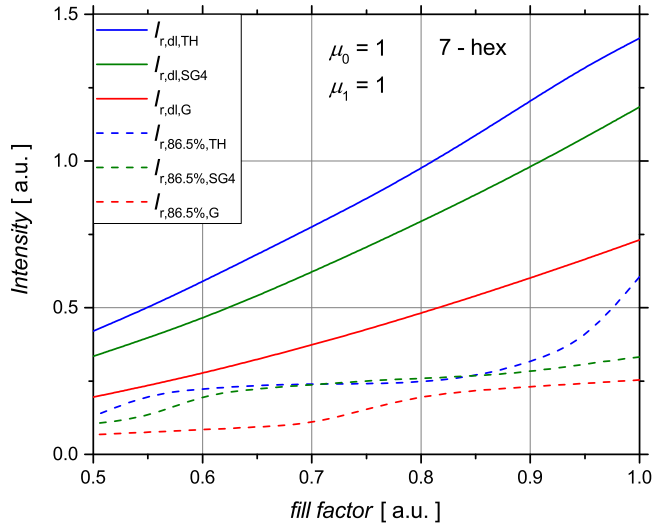

Fig. 6. Averaged intensities in the diffraction limit and $\mathrm{PIB}_{86.5\%}$ vs filling factor, for three profiles ($p = 0,\ 1,\ 4$), 7-hex.

- PIB_{dl} , which is the combining efficiency, defined as a diffraction-limited PIB_{dl} in the arbitrarily taken diffraction limit $\alpha_{\mathrm{dl}} = 0.75$, corresponding to $2\theta_{\mathrm{dl}} = 1.5\lambda/D$:

$$PIB_{dl} = PIB(\alpha_{dl}) \tag{19}$$

- $I_{r,dl}$, corresponding to the relative averaged intensity in the diffraction limit:

$$I_{r,dl} = PIB(\alpha_{dl})/\alpha_{dl}^2 \tag{20}$$

- $I_{r,86.5\%}$, corresponding to the relative intensity inside a circle with radius $\alpha_{86.5\%}$:

$$I_{r,86.5}\% = 0.865/\alpha_{86.5}\%^2 \tag{21}$$

where $\alpha_{86.5\%}$, corresponding to the typical definition of the laser beam diameter [24], satisfies the following equation:

$$PIB(\alpha_{86.5\%}) = 0.865 \tag{22}$$

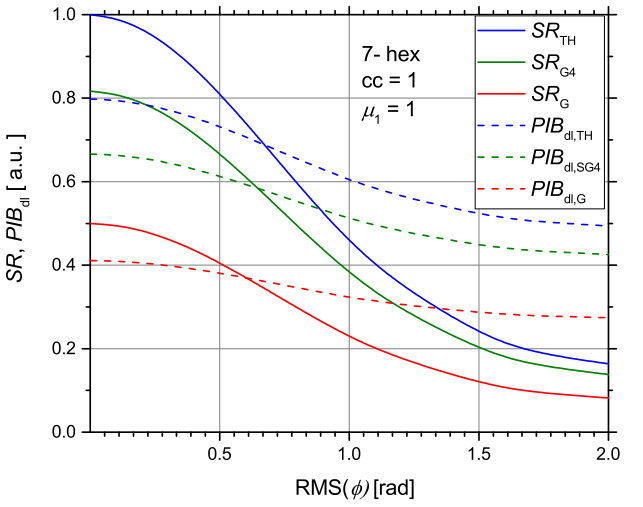

Fig. 7. Strehl ratio SR, combining efficiency PIB_{dl} vs the RMS phase mismatch error for three profiles ($p = 0,\ 1,\ 4$); 7-hex.

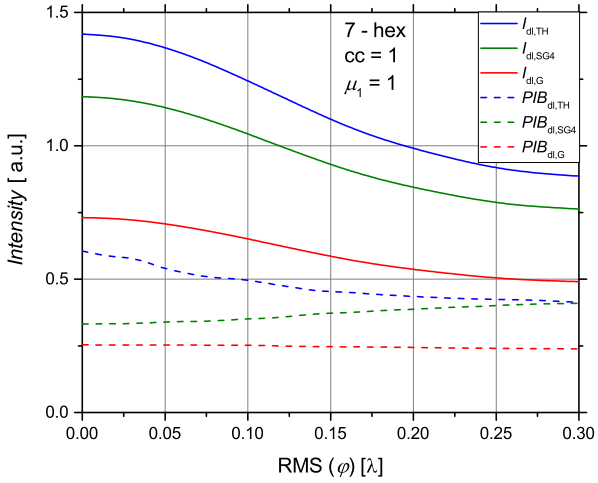

Fig. 8. Averaged intensities in the diffraction limit and $\mathrm{PIB}_{86.5\%}$ vs. RMS phase mismatch error for three profiles ($p = 0,\ 1,\ 4$), 7-hex.

3. Impact of geometry, beam profile, and filling factor on the CBC performance

In the case of full coherence ($\mu_0 = \mu_1 = 1$), the Strehl ratio SR can be calculated taking into account only the intensity of a single emitter in the far field. Let us note that a change in the filling factor c results in the "stretching" of the far field intensity distribution determined for the given beam profile (p), not influencing the second component. To calculate the remaining performance metrics, the second component in Eq. (9) has to be calculated and the PIB values for each case have to be computed as well. The 2D maps of intensity distribution in logarithmic scale (Fig. 2 a, b, c) show the structures of diffraction patterns in far field for three cases of coherently combined arrays ($p = 0,\ 4,\ 1$) with filling factor c=1. The green/blue rounds in Fig. 2 correspond to the local minima between diffraction orders and the inserted dashed circle defines the 1.5λ/D diffraction limit border.

The differences in the far field between the three beam profiles ($p = 0,\ p = 4,\ p = 1$) are presented in Figs. 3 and 4.

The performance metrics presented in Table 1 were determined according to Eqs. (17)–(21).

In the next step, we have calculated the impact of the filling factor for several beam profiles, for the fully coherent case (Figs. 5 and 6).

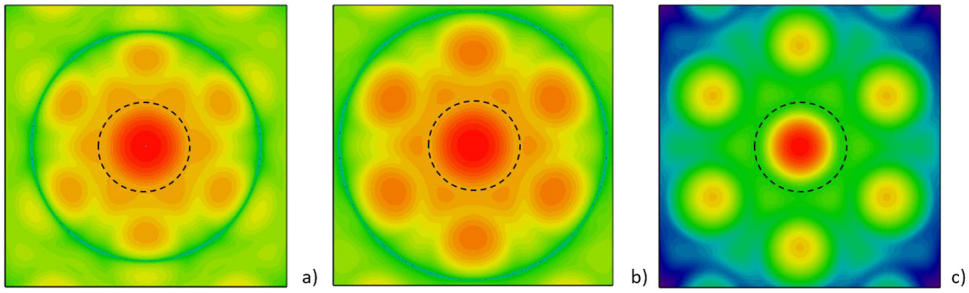

Fig. 9. 2D intensity distributions in logarithmic scale in the far field for (a) $p = 0$, (b) $p = 4$, (c) $p = 1$. For $\mu_0 = 1$, $\mu_1 = 0.85193$, the dashed circles show the diffraction limit at $1.5\lambda/D$.

Table 1
CBC performance metrics for 7 and 19 hexagonal lattices, filling factor $c = 1$, $\mu_0 = \mu_1 = 1$. The values of w_0, w_1 and w_4 were determined according to formulas (2, 3) assuming truncation losses $\varepsilon < 0.001$.

	"top hat"; $p = 0$, w_0=1		SuperGauss $p = 4$, $w_4 = 0.8929$		Gauss; $p = 1$; $w_1 = 0.5$	
	7-hex	19-hex	7- hex	19-hex	7-hex	19-hex
SR	1	1	0.841	0.841	0.502	0.502
PIB_{dl}	0.8052	0.8035	0.6589	0.6523	0.3981	0.3868
$I_{r,dl}$	1.8566	1.7669	1.5179	1.4339	0.9167	0.8602
$I_{r,86.5\%}$	0.7670	0.7123	0.3392	0.1127	0.2572	0.0953

As shown in Figs. 5 and 6, performance increases with increasing the filling factor. For a technically feasible filling factor c = 0.9, performance drops to ~80% of maximum, for each case. Let us note that the metrics based on 86.5% of PIB $I_{r,86.5}$ are ambiguous, and do not change significantly with the filling factor, mainly owing to the flattened shape of the PIB curve at the edge of the range (Figs. 3 and 4).

4. Impact of partial coherence on CBC performance

4.1. Impact of phase mismatch in the near field

The phase mismatch error defined by Eqs. (17) and (18) generally negatively affects all of the performance metrics (Figs. 7 and 8) in a nonlinear way.

We conclude that the effect is similar to the one in the case of a single "*top hat*" aperture. We take $SR = 80\%$ RMS phase error as $\sim 0.07\lambda$ (Fig. 7), consistent with the Marechal criterion for a full aperture with a homogeneous intensity profile.

4.2. Impact of space dependent phase error according to "5/3 index law"

We have analyzed the influence of the coherence radius on the performance metrics assuming the "5/3 *index law*" of partial coherence (Eqs. (11)–(13)). Let us consider firstly the 2D distributions for the partial coherence case with $\mu_1 = 0.85193$, corresponding to $\rho_0/D = 1/3$ (Fig. 9).

The SR changes significantly (Fig. 10) for a full range of coherence radii. The combining efficiency, defined by PIB_{dl} and the intensity, does not change noticeably for coherence radii larger than the aperture. The reduction to 80% of maximum corresponds to the case of ρ_0/D_{aper} approximately equal to 1/3, i.e., to the ratio of coherence radius to the sub-aperture diameter.

Similar to the case of space-invariant phase error (p. 4.1), the performance metrics defined at 86.5% of PIB (Fig. 11) are not noticeably affected by coherence changes. Thus, we conclude that there is no significant difference between CBC and ICBC when the far field diameter is defined according to the criterion of 86.5% of PIB.

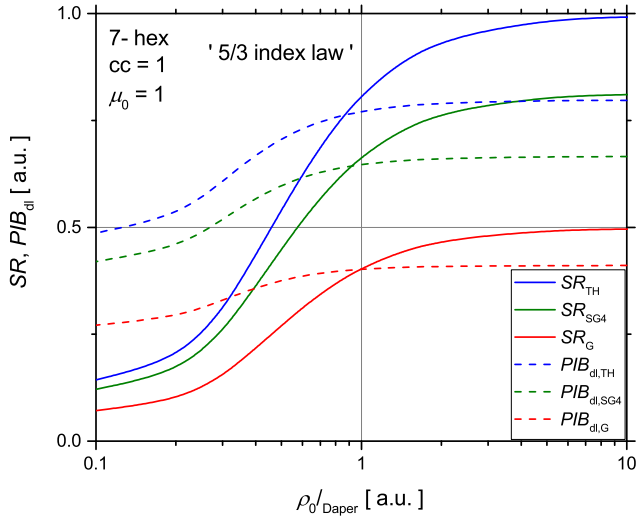

Fig. 10. Strehl ratio SR, combining efficiency PIB_{dl} vs ratio of coherence radius to aperture ρ_0/D_{aper}, for three profiles ($p = 0$, 1, 4); 7-hex.

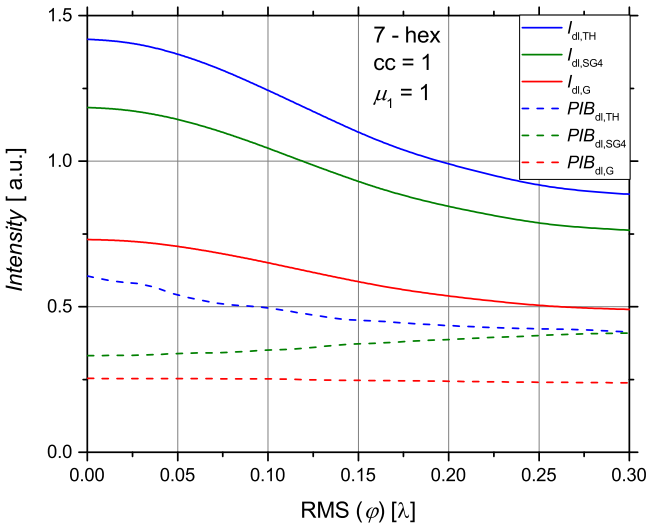

Fig. 11. Averaged intensities in the diffraction limit and $PIB_{86.5\%}$ vs ratio of coherence radius to aperture ρ_0/D_{aper} for three profiles ($p = 0$, 1, 4); 7-hex.

5. Conclusions

Dependence of the CBC performance metrics on several factors, such as the beam profile, filling factor, and change in the partial space coherence, was studied in this work. We have shown that the performance metrics based on 86.5% of PIB are not noticeably affected

by changes in the beam profile, filling factor, or partial coherence; thus, they are not adequate measures of the CBC quality. In other words, there is no noticeable difference between ICBC and CBC in terms of the far field diameter based on the $PIB_{86.5}$ definition.

On the other hand, Strehl's ratio is an "artificial" mathematical parameter, does not have precise experimental analogue, and does not reflect the interaction of the laser beam with a target. Thus, it, too, is not an adequate metric for estimating the CBC system performance.

In our opinion, the adequate metrics for the analysis of CBC systems are those based on the diffraction limit. We have taken here as a diffraction limit 0.75λ/D, which corresponds to the "*full aperture top hat*" case, with the content near 85% of power.

As a rule, the beam intensity in the far field is in a nearly quadratic dependence on the filling factor, which dominates other effects. The filling factor of 90% seems to be feasible.

We conclude that the impact of the beam profile is important. It was shown that the combining efficiency and intensity drops more than two times for a Gaussian profile compared with the "*top hat*" one. A reasonable compromise is a SG_4 profile, for which intensity drops to ~83% of the "*top hat*" case, which is more than 160% larger compared with the Gaussian case.

The analysis of the influence of space-invariant phase mismatch errors yielded similar results as in the case of single-aperture optics with the "*top hat*" distribution. The decrease to 80% of the maximum approximately corresponds to the RMS phase error of 0.07λ, which is consistent with the Marechal criterion.

The most interesting are the results of the calculation performed for the "*5/3 index law*" of partial coherence (according to the Kolmogorov model of atmospheric turbulence, [21,22]). For a weak decrease in coherence (defined here as $\rho_0/D_{\text{aper}} > 1$) the effect of such defined partial coherence can be neglected. The limit of the accepted level of partial coherence (causing a decrease to 80% of the performance metric PIB_{dl}) corresponds roughly to $\rho_0/D_{aper} \sim 1/3$, i.e., to $\rho_0/2a \sim 1$.

The final conclusion is that CBC makes sense for beams with profiles similar to the super-Gaussian ones with the index $p = 4$ and the RMS phase mismatch error of 0.07 wavelength. Such requirements can be in principle satisfied in future CBC systems by exploiting a precise control of phase mismatch between emitters and beam-shaping technologies. The control and compensation of turbulence to the level of $\rho_0/D_{aper} > 1/3$ seems to be the main challenge for adaptive optics destined for CBC systems.

The proposed approach and the obtained results could be used for constructing new types of CBC systems. The phase error analysis can be used for defining requirements on maximal admissible errors of compensation systems.

Acknowledgment

The work was financed in the framework of strategic program DOB-1-6/1/PS/2014 financed by the National Centre for Research and Development of Poland.

References

[1] G.P. Perram, S.J. Cusumano, R.L. Hengelhold, S.T. Fiorino, An Introduction to Laser Weapon Systems, Directed Energy Professional Society, Albuquerque, NM, 2010.
[2] H. Injeyan, S. Palese, G.D. Goodno, High Power Laser Handbook, Mc Graw Hill, New York, 2011.
[3] R.A. Motes, S.A. Shakir, R.W. Berdine, Introduction to High Power Lasers, Directed Energy Professional Society, Albuquerque, NM, 2013.
[4] P. Sprangle, B. Hafizi, A. Tino, R. Fischer, High-power lasers for directed-energy applications, Appl. Opt. 54 (31) (2015) F201–F206.
[5] D.C. Brown, Ultrahigh-average-power diode-pumped Nd:YAG and Yb:YAG lasers, J. Quantum Electron. 33 (5) (1997) 861–873.
[6] M.N. Zervas, C.A. Codemard, High power fiber lasers: A review, J. Sel. Top. Quantum Electron. 20 (2014) 0904123.
[7] J.W. Dawson, M.J. Messerly, R.J. Beach, M.Y. Shverdin, E.A. Stappaerts, A.K. Sridharan, P.H. Pax, J.E. Heebner, C.W. Siders, C.P.J. Barty, Analysis of the scalability of-diffraction-limited fiber lasers and amplifiers to high average power, Opt. Express (2008) 13240–13266, 16917.
[8] S.J. McNaught, H. Komine, S.B. Weiss, R. Simpson, A.M. Johnson, J. Machan, C.P. Asman, M. Weber, G.C. Jones, M.M. Valley, A. Jankevics, D. Burchman, M. McClellan, J. Sollee, J. Marmo, H. Injeyan, 100 kW coherently combined slab MOPAs, in: Conference on Lasers and Electro-Optics/International Quantum Electronics Conference, in: OSA Technical Digest (CD) (Optical Society of America, 2009), Paper CThA1, 2009.
[9] https://www.ipgphotonics.com/en/products/lasers/high-power-cw-fiber-lasers/1-micron/yls-sm-1-10-kw.
[10] B.V. Zhdanov, R.J. Knize, Review of alkali laser research and development, Opt. Eng. 52 (2) (2013) 021010-1 – 021010-8.
[11] G.A. Pitz, D.M. Stalnaker, E.M. Guild, B.Q. Oliker, P.J. Moran, S.W. Townsend, D.A. Hostutler, Advancements in flowing diode pumped alkali lasers, Proc. SPIE 9729 (2016) 972902.
[12] T.Y. Fan, Laser beam combining for high-power, high-radiance sources, IEEE J. Sel. Top. Quantum Electron. 11 (3) (2005) 567–577.
[13] B. Arnaud, A. Brignon, Coherent Laser Beam Combining, Wiley-VCH Verlag GmbH & Co., Weinheim, 2013.
[14] E. Honea, R.S. Afzal, M. Savage-Leuchs, J. Hennie, K. Brar, N. Kurz, D. Jander, N. Gitkind, D. Hu, C. Robin, A.M. Jones, R. Kashnadhuni, R. Humphreys, Advances in fiber laser spectral beam combining for power scaling, Proc. SPIE 9730 (2016) 97300Y.
[15] Y. Li, L. Qian, D. Lu, D. Fan, S. Wen, Coherent and incoherent combining of fiber array with hexagonal ring distribution, Opt. Laser Technol. 39 (2007) 957–963.
[16] G.D. Goodno, C.-C. Shih, J.E. Rothenberg, Perturbative analysis of coherent combining efficiency with mismatched lasers, Opt. Express 18 (24) (2010) 25403–25414.
[17] P. Sprangle, J. Penamo, R. Fischer, B. Hafizi, Incoherent combining and atmospheric propagation of high-power fiber lasers for directed-energy applications, IEEE J. Quantum Electron. 45 (2) (2009) 138–148.
[18] K. Ludweigt, T. Riesbeck, A. Graf, M. Jung, 50 kW laser weapon demonstrator of rheinmetall waffe munition, Proc. SPIE 8898 (2013) 88980N.
[19] https://www.mbdacareers.co.uk/news-media/mbda-blog/high-energy-laser-weapons.
[20] https://commons.wikimedia.org/wiki/File:Laser_Weapon_System_(LaWS)_demonstration_aboard_USS_Ponce.webm.
[21] J.W. Goodman, Introduction to Fourier Optics, John Wiley & Sons, New York, 1985.
[22] L. Andrews, R.L. Philips, Laser Beam Propagation Through Random Media, SPIE Press, Bellingham, WA, 1998.
[23] I. Toselli, S. Gladysz, On the general equivalence of the fried parameter and coherence radius for non-Kolmogorov and oceanic turbulence, OSA Contin. 2 (2019) 43–48.
[24] J.W. Goodman, Statistical Optics, John Wiley & Sons, New York, 1985.
[25] T. Sean Ross, Laser Beam Quality Metrics, in: Tutorial Text TT96, SPIE Press, Bellingham, 2013.